

HYDROGEN PRODUCTION FROM METHANE CRACKING IN DIELECTRIC BARRIER DISCHARGE CATALYTIC PLASMA REACTOR USING A NANOCATALYST

Khoja AH, Azad AK, Saleem F, Khan BA, Naqvi SR, Mehran
MT, Amin NAS

Bibliographic citation

Khoja, A. H., Azad, A. K., Saleem, F., Khan, B. A., Naqvi, S. R., Mehran, M. T., & Amin, N. A. S. (2020). Hydrogen production from methane cracking in dielectric barrier discharge catalytic plasma reactor using a nanocatalyst. *Energies*, 13(22), 5921.

Link to Published Version: <https://doi.org/10.3390/en13225921>

If you believe that this work infringes copyright, please provide details by email to acquire-staff@cqu.edu.au

aCQUIRe CQU repository






This is an open access article under [Creative Commons](#) license.

Downloaded on 19/01/2023

Please do not remove this page

Article

Hydrogen Production from Methane Cracking in Dielectric Barrier Discharge Catalytic Plasma Reactor Using a Nanocatalyst

Asif Hussain Khoja ^{1,*}, Abul Kalam Azad ^{2,*}, Faisal Saleem ³, Bilal Alam Khan ⁴,
Salman Raza Naqvi ⁵, Muhammad Taqi Mehran ⁵ and Nor Aishah Saidina Amin ⁶

¹ Fossil Fuels Laboratory, Department of Thermal Energy Engineering, US-Pakistan Centre for Advanced Studies in Energy (USPCAS-E), National University of Sciences & Technology (NUST), Sector H-12, Islamabad 44000, Pakistan

² School of Engineering and Technology, Central Queensland University, 120 Spencer Street, Melbourne 3000, VIC, Australia

³ Department of Chemical and Polymer Engineering, University of Engineering and Technology, Lahore 38000, Faisalabad Campus, Pakistan; h.faisalsaleem@gmail.com

⁴ Department of Applied Science and Technology, Politecnico di Torino, Corso Duca degli Abruzzi, 24, 10129 Torino, Italy; bilal.khan@polito.it

⁵ School of Chemical and Materials Engineering, National University of Sciences & Technology (NUST), Sector H-12, Islamabad 44000, Pakistan; salman.raza@scme.nust.edu.pk (S.R.N.); taqimehran@scme.nust.edu.pk (M.T.M.)

⁶ Chemical Reaction Engineering Group, School of Chemical & Energy Engineering, Faculty of Engineering, University Technology Malaysia (UTM), Skudai, Johor Bahru 81310, Malaysia; noraishah@cheme.utm.my

* Correspondence: asif@uspcase.nust.edu.pk (A.H.K.); a.k.azad@cqu.edu.au (A.K.A.); Tel.: +92-51-8865343 (A.H.K.)

Received: 9 October 2020; Accepted: 11 November 2020; Published: 13 November 2020



Abstract: The study experimentally investigated a novel approach for producing hydrogen from methane cracking in dielectric barrier discharge catalytic plasma reactor using a nanocatalyst. Plasma-catalytic methane (CH_4) cracking was undertaken in a dielectric barrier discharge (DBD) catalytic plasma reactor using $\text{Ni/MgAl}_2\text{O}_4$. The $\text{Ni/MgAl}_2\text{O}_4$ was synthesised through co-precipitation followed customised hydrothermal method. The physicochemical properties of the catalyst were examined using X-ray diffraction (XRD), scanning electron microscopy—energy dispersive X-ray spectrometry (SEM-EDX) and thermogravimetric analysis (TGA). The $\text{Ni/MgAl}_2\text{O}_4$ shows a porous structure spinel MgAl_2O_4 and thermal stability. In the catalytic-plasma methane cracking, the $\text{Ni/MgAl}_2\text{O}_4$ shows 80% of the maximum conversion of CH_4 with H_2 selectivity 75%. Furthermore, the stability of the catalyst was encouraging 16 h with CH_4 conversion above 75%, and the selectivity of H_2 was above 70%. This is attributed to the synergistic effect of the catalyst and plasma. The plasma-catalytic CH_4 cracking is a promising technology for the simultaneous H_2 and carbon nanotubes (CNTs) production for energy storage applications.

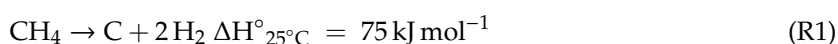
Keywords: hydrogen production; methane cracking; DBD plasma reactor; MgAl_2O_4 ; CNTs

1. Introduction

The atmosphere is heavily polluted due to the urbanisation and commercialisation throughout the globe. It causes serious greenhouse gases (GHGs) emissions, more specifically, the carbon dioxide (CO_2) and methane (CH_4) along with other volatile compounds. Various techniques have been applied to treat the GHGs to reduce harmful emissions for sustainable development. One of the exciting techniques is to utilise the GHGs for producing zero-emission fuel, which is currently under

investigation throughout from the last couple of decades. It is an essential step to reduce the GHG concentration in the atmosphere as well as a sustainable approach for fuel synthesis [1–3]. Previous studies revealed that CH₄ is one of the prominent components of GHG with a total share of 16% in the environment usually emitted from petroleum processing, waste management and agriculture activities [4].

On the other hand, CH₄ is also the principal constituent (76 wt%) of natural gas (NG) which reserves are abundantly available in underground. The utilisation of CH₄ has various routes as fuel both in domestic and industrial processes. One of the most sustainable and attractive ways to utilise CH₄ is to produce syngas and hydrogen (H₂) along with co-reactants such as O₂, H₂O, and CO₂ [5,6]. The popular routes for CH₄ mitigation are thermocatalytic processes such as thermal decomposition of methane as shown in the below reaction (R1), methane partial oxidation [7], methane dry reforming [8–10] and methane steam reforming [11] in thermal reactors. The higher energy input for elevated temperatures makes the thermal reactors economically challenging for this process [12,13]. Various techniques have been employed to overcome the shortfalls to make the process viable [14,15].



In recent days, various plasma systems are used for the processing of the methane cracking as well as other oxidative reactions using microwave plasma, spark plasma [8,10,16] and nonthermal plasmas (NTPs) like dielectric barrier discharge (DBD) and silent discharges. NTP seeks attention for gas processing, especially the DBD cold plasma reactor is one of the promising techniques [8,12]. The DBD plasma reactor has some useful characteristics from low-temperature operation to accessible upscaling opportunities as compared to thermal plasma [8,17]. More significant aspects of the DBD plasma for gas processing has been reported in an extensive review by Ramses and Bogaerts [12]. In addition, the DBD plasma has been successfully utilised for CH₄ cracking with efficient conversion and significant H₂ yield [18–20]. The hydrogen is the next-generation future fuel due to the recent developments in hydrogen-based fuel cell technologies [21]. The DBD plasma-based methane cracking has been reported in several studies aiming for cleaner production of H₂. However, the conversion efficiency and cleaner H₂ is always challenging in the DBD plasma reactor for a longer time on streams [6,22].

To improve the conversion of CH₄, the various catalysts have been employed in the catalytic DBD plasma. The most valuable catalysts for plasma catalytic DBD methane cracking are Ni/γ-Al₂O₃, γ-Al₂O₃, Pd/SiO₂, Pd/TiO₂, Pd/Al₂O₃ [23], Pt/γ-Al₂O₃ [24], ZnO, ZnCr₂O₄, Cr₂O₃ [25]. The improvement in the conversion of CH₄ as well as enhanced product selectivity been a witness in various referenced studies [25]. Plasma-catalysis drives scope on improving the selectivity of targeted products which is very important for CH₄ cracking process. The magnesium aluminate (MgAl₂O₄) as a catalyst has been investigated for various reforming process [9,26,27] as well as plasma catalytic methane dry reforming in previous studies. It demonstrated a substantial improvement in conversion of reactants and product distribution, especially on the H₂ selectivity [28,29]. The nickel (Ni) impregnated MgAl₂O₄ can improve the CH₄ conversion and H₂ selectivity suppressing the recombination of methyl radicals [30]. The MgAl₂O₄ based catalyst has not been previously reported as its distinct properties such as high resistance to temperature, and mild plasma conditions are much suitable to use in plasma-based methane cracking processes. Therefore, it is seems meaning to incorporate the Ni impregnated MgAl₂O₄ in the DBD plasma reactor for methane cracking for hydrogen production and simultaneously it produces carbon nanotubes (CNTs) which are essential material for energy storage applications [31]. Plasma produces a very clean and well-structured CNTs for further application reported in various studies.

In this work, an experimental study has been conducted to the synthesis of a nanocatalyst (Ni/MgAl₂O₄) for CH₄ cracking in fixed bed DBD plasma reactor for H₂ and CNTs production. The catalyst was synthesised using the co-precipitation method followed by hydrothermal process. The catalyst is further characterised by X-ray diffraction (XRD), scanning electron microscopy (SEM), energy dispersive X-ray spectrometry (EDX) and thermogravimetric analysis (TGA). Furthermore,

the stability of the catalyst was examined for 16 h reaction time or time on stream (TOS). Finally, spent catalyst is further characterised using SEM, TGA and differential thermogravimetric (DTG) to investigate the formed CNTs over catalyst surface.

2. Materials and Methods

2.1. Synthesis of Ni/MgAl₂O₄

The support MgAl₂O₄ was prepared through co-precipitation process supported by the hydrothermal method presented in Figure 1. Briefly, magnesium nitrate hexahydrate (Mg(NO₃)₂·6H₂O) (99.5 %, Sigma, St. Louis, MI, USA) and aluminium nitrate nonahydrate (Al(NO₃)₃·9H₂O) (99.5 %, Merck, NJ, USA) was dissolved in ACS reagent, ammonia solution (28.0%) with the 2:1 molar ratio of Mg:Al. The nitrate solution was then combined to 0.01 molar citric acid (CA) solution using pipette at 60 °C on continuous stirring at a speed of 350 rpm. The ammonia is acting as a precipitating agent while citric acid is assisting control crystal growth and morphology. The nitrate solution is transferred to a polytetrafluoroethylene (PTFE) Teflon autoclave and kept in the furnace for 24 h at a temperature of 160 °C. Further, the sample has been washed using ethanol numerous times and deionised (DI) water for the removal of impurities. The prepared samples dried in the oven at a temperature of 120 °C for 24 h to remove the moisture. The received derived sample was crushed and kept for calcination at 700 °C for 4 h.

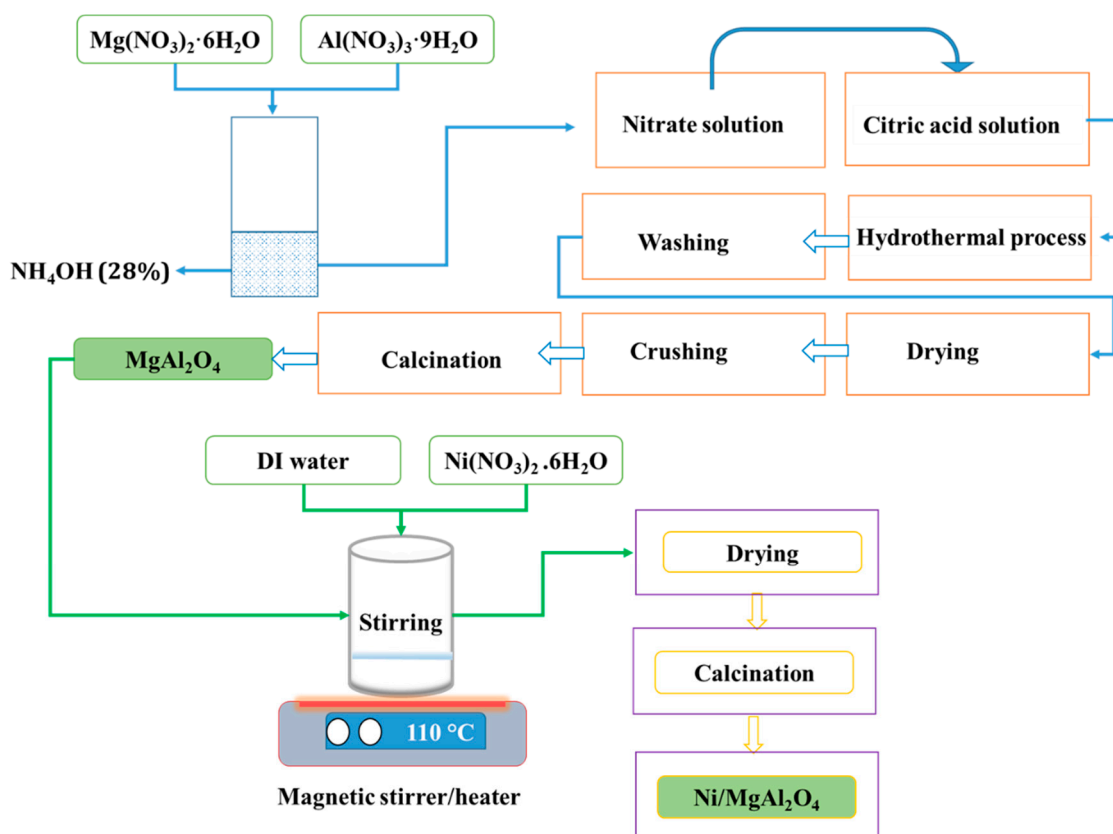


Figure 1. Schematic of Ni/MgAl₂O₄ synthesis.

For Ni impregnation, wetness incipient impregnation technique has been employed. The precursor (10 wt%), nickel nitrate hexahydrate (Ni(NO₃)₂·6H₂O) (99%, Merck) was added to DI water to get 0.01 molar nitrate solution. The nitrate solution stirred for 10 min at 60 °C. The required amount of support MgAl₂O₄ was then combined to the nickel nitrate solution and stirring for three (3) hours at 110 °C. The sample was kept in a furnace (CSF 1100, Carbolite, Cheshire, UK) for overnight about 10 to 12 h

for drying. The dried sample was crushed and preserved in the furnace for 5 h at 700 °C to achieve the final catalyst for methane cracking application.

2.2. Materials Characterisation

The physicochemical properties of the synthesised catalyst are examined by several methods i.e., XRD, SEM-EDX and TGA. XRD was accomplished employing Bruker's X-ray Diffractometer (D8-Advance, MA, USA), using Cu- α radiation (40 kV, 200 mA). The crystallite size was analysed by Scherrer's equation [32]. After that, SEM was carried out using TESCAN VEGA 3 (Czech Republic), conducted at 20 kV HV and integrated with the beam of X-MaxN by Zeiss optics [13]. TGA 5500 (TA Instruments, Newcastle, DC, USA) was used to analyse the weight loss (%) and differential thermogravimetric analysis (DTG) of the fresh catalyst. The sample (10 mg) was loaded in a platinum pan and placed in the furnace at a heating rate of 10 °C min⁻¹ under the N₂ flow of 40 mL min⁻¹ [30,33]. Spent catalyst was characterised by SEM and TGA-DTG ((TA Instruments, Newcastle, DC, USA)) after 16 h TOS to investigate the morphological changes and CNT formation.

2.3. Plasma-Catalytic Methane Cracking System

The experimental setup for the catalytic-DBD reactor for CH₄ cracking is as shown in Figure 2. The reactant CH₄ (99.9 %) flow rate was regulated by a mass flow meters/controller (MFC) (Alicat, Tucson, AZ, USA). The plasma power supply model CTP-2000K (Nanjing, China) incorporated with the high voltage regulator was used to produce plasma in the DBD reactor. The input voltage and input current were also monitored by Tektronix TDS 2012B oscilloscope (Beaverton, OR, USA) coupled with voltage probe Tek P6015A (Beaverton, OR, USA) [28]. The plasma reactor consists of an alumina tube having an inner diameter (ID) of 10 mm and the outer diameter (OD) of 12 mm. The stainless steel rod with an inner diameter of 4 mm and 20 cm in length was utilised as a HV electrode while a mesh of aluminium is wrapped serving as a ground electrode. The prepared catalyst is loaded in the centre of the alumina tube hold by quartz wool. The gases were analysed by GC-TCD/FID (Agilent 6890N, Santa Clara, CA, USA). The GC column details are given in details here [34]. The HP PlotQ capillary column with configuration of 40 m × 0.53 mm ID, 40 µm was used to detect CO₂ while Molsieve column with the configuration of 30 m × 0.530 mm ID, 25 µm used for detecting H₂ and CH₄, both the columns were connected to TCD. Another column HayeSep Q-Supelco with the configuration of 6 ft × 1/8 in. ID × 2.1 mm OD, 80/100 mesh was employed as TCD C₂–C₆ back flashing. To separate the hydrocarbons ranging from C₁–C₆ were analysed by GS-Gaspro column having the configuration of 60 m × 0.32 mm ID) detected to FID. Agilent supplied all the columns. The process parameters such as feed flow rates, power input and loading of prepared catalyst were maintained constant.

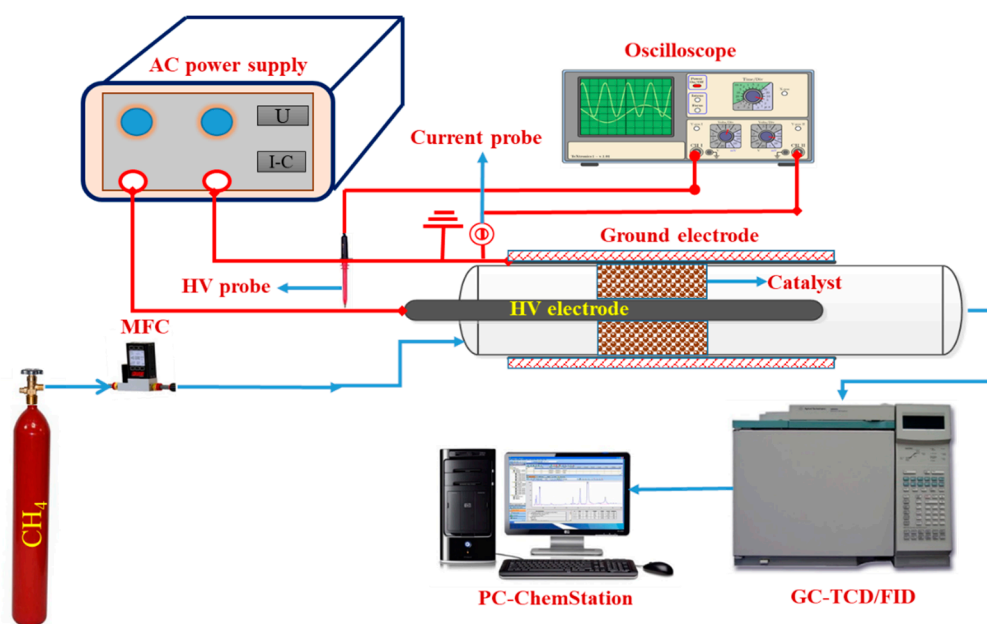


Figure 2. Schematic of fixed bed DBD catalytic-plasma reactor setup for methane cracking.

The plasma-catalytic performance was monitored for methane conversion, H_2 selectivity, specific input energy (SIE) and DBD energy efficiency (EE) using the following equations (Equations (1)–(4)).

$$CH_4 \text{ conversion } (X_{CH_4})\% = \left[\frac{(n_{CH_4})_{\text{converted}}}{(n_{CH_4})_{\text{feed}}} \times 100 \right] \quad (1)$$

$$H_2 \text{ selectivity } (S_{H_2})\% = \left[\frac{(n_{H_2})_{\text{produced}}}{(2 \times n_{CH_4})_{\text{conversion}}} \times 100 \right] \quad (2)$$

$$SIE \left(\frac{J}{mL} \right) = \left[\frac{P_{in} (J \text{ sec}^{-1})}{\text{Total feed flow rate } (mL \text{ min}^{-1})} \right] \times \frac{60 \text{ sec}}{1 \text{ min}} \quad (3)$$

$$EE \left(\frac{mmol}{kJ} \right) = \left[\frac{(n_{CH_4} + n_{CO_2})_{\text{converted}} (mmol \text{ min}^{-1})}{P_{in} (kJ \text{ min}^{-1})} \right] \quad (4)$$

where n = molar fraction of the gases. Feed flow rate was quantified in $mL \text{ min}^{-1}$ was transformed into $mmol \text{ min}^{-1}$ applying the conditions; temperature $T = 25^\circ \text{C}$, $p = 1 \text{ atm}$ along with a conversion factor, $1 \text{ mmol} = 24.04 \text{ mL}$ [34]. The calculation of the P_{in} calculation is reported elsewhere [34]. The experiments were replicated to minimise experimental errors.

3. Results and Discussion

3.1. Physicochemical Properties of the Catalyst

Figure 3 illustrates the XRD pattern for synthesising $MgAl_2O_4$ and 10 wt% $Ni/MgAl_2O_4$. The $MgAl_2O_4$ spinel is identified for the JCPDS# 72-6947, showing a single spinel cubic phase and prominent peaks are found at 19° (111), 37° (220), 38.7° (311), 44.9° (400), 55.9° , 59.6° and 65.5° (440), and are in good agreement with the literature [35]. It also shows the space group (227:Fd-3m), the crystallite sized (average) is recorded at 10.3 nm. In addition, hexagonal structure NiO is detected for the JCPDS # 44-1159 having major peaks at 37.5° , 43.9° and 63° with miller indices of (101), (012) and (110) correspondingly [36]. The space group for hexagonal NiO is R-3m(166) and active phase is NiO^{2+} [37].

The crystallite size is 9.7 nm for NiO, and the finer crystallite size depicts the formation of a uniform structure catalyst and dispersion over support MgAl_2O_4 .

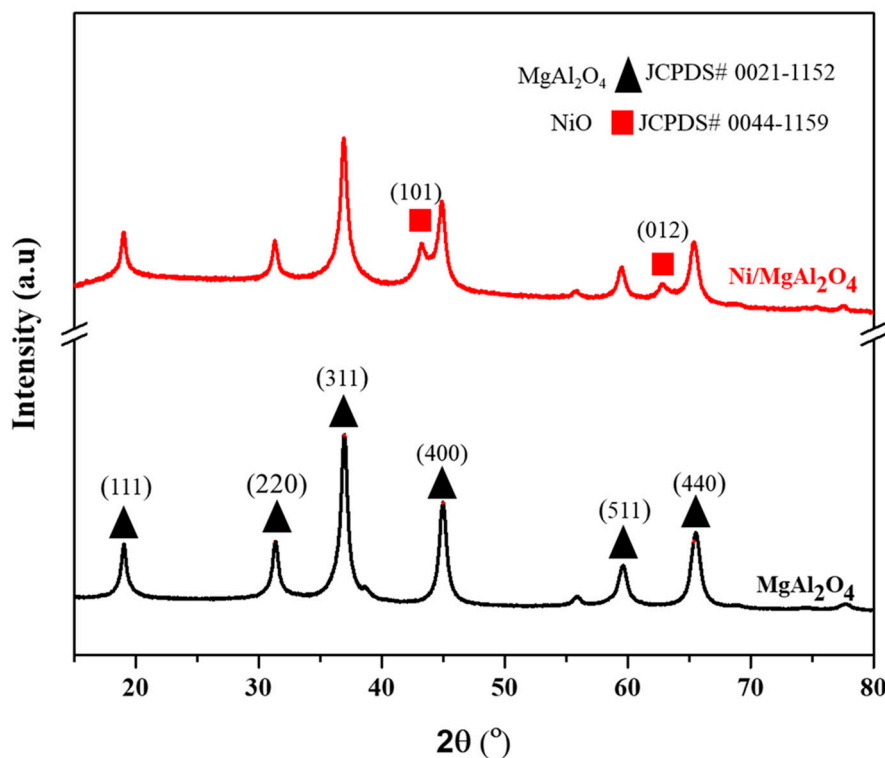


Figure 3. XRD pattern of synthesized MgAl_2O_4 and $\text{Ni/MgAl}_2\text{O}_4$.

The surface morphology of MgAl_2O_4 and $\text{Ni/MgAl}_2\text{O}_4$ is examined using the SEM with magnifications of 5 μm and 500 nm and presented in Figure 4. The MgAl_2O_4 shows the fine particles with spherical structure, and some particles exhibited the worm-like shapes Figure 4a,b [38]. The two different morphologies of the MgAl_2O_4 offers a comprehensive and uniform distribution of Ni over the surface depicted in Figure 4c,d. The porous structure of MgAl_2O_4 offers to diffuse the Ni inside the pores and create actives sites. It may also assist the reactant gas and plasma species interaction later in the plasma-catalytic process.

The elemental analysis of MgAl_2O_4 and 10 wt% $\text{Ni/MgAl}_2\text{O}_4$ are demonstrated in Figure 5a,b. The significant elements O, Mg and Al, were found, and the composition is exhibited inset table and spectrum of Figure 5a. While 10 wt% $\text{Ni/MgAl}_2\text{O}_4$ shows Ni along with O, Al and Mg, which is evident in the presence of Ni in the reported catalyst. The extra peaks without identification are due to the carbon tape and gold coating before the SEM/EDX analysis.

The TGA for 10 wt% $\text{Ni/MgAl}_2\text{O}_4$ is undertaken to analyse the thermal stability of the prepared samples, as shown in Figure 6. The 6% weight loss under 300 $^{\circ}\text{C}$ is observed, and it is ascribed to the moisture and volatile matters depicted in Figure 6, column A. In column B, which temperature is more significant than 300 $^{\circ}\text{C}$ demonstrated no weight loss further to 900 $^{\circ}\text{C}$. This analysis revealed that the synthesised catalyst is stable for the plasma-catalytic operation for methane cracking in mild conditions [39]. The unstable catalyst may lead to phase modification and sintering later in the methane cracking reactions [40].

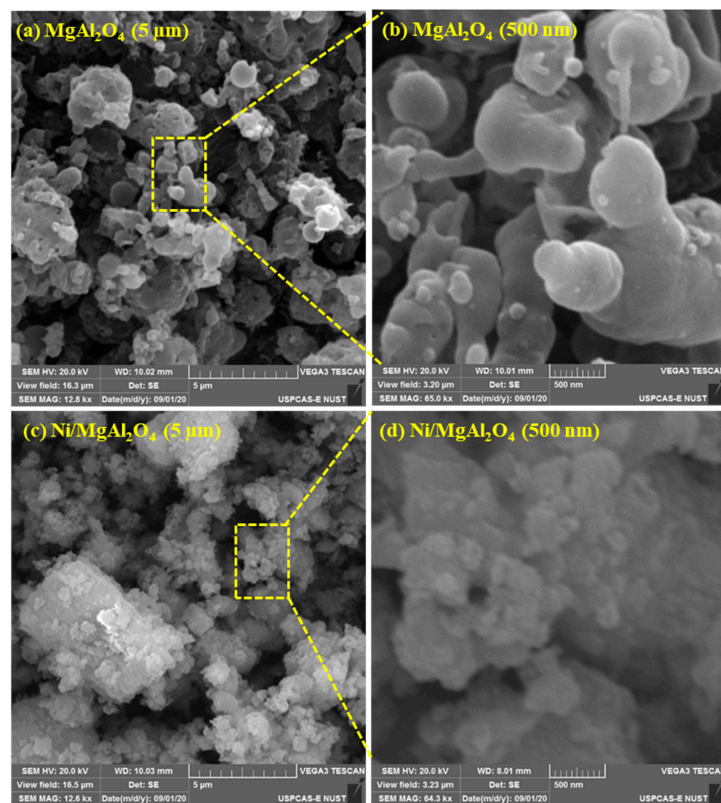


Figure 4. SEM micrograph of synthesised fresh samples; (a,b) MgAl_2O_4 (c,d) 10 wt%Ni/ MgAl_2O_4 having 5 μm and 500 nm of magnification.

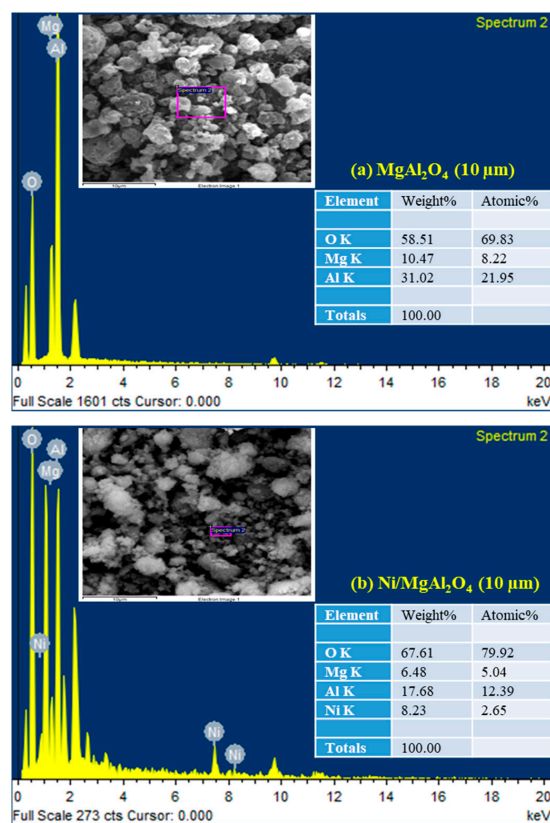


Figure 5. (a) EDX elemental analysis of (a) MgAl_2O_4 (b) 10 wt% Ni/ MgAl_2O_4 of using point ID technique.

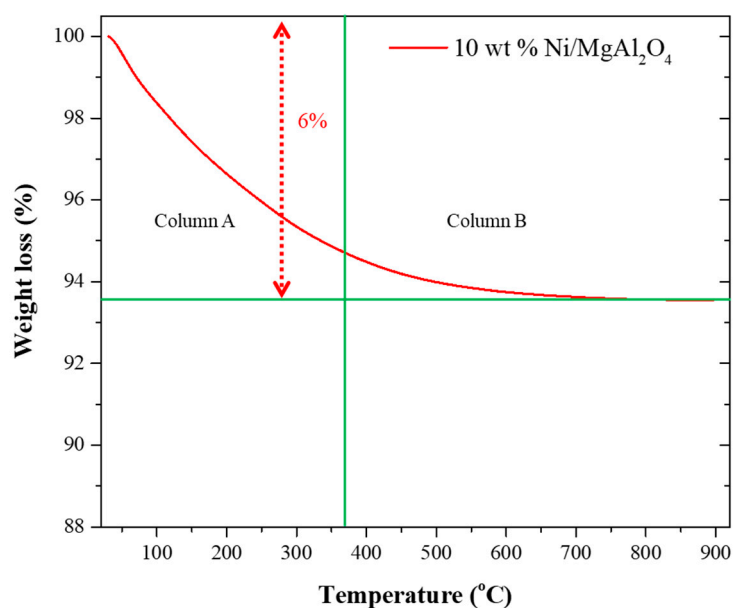


Figure 6. TGA analysis of fresh 10 wt% Ni/MgAl₂O₄.

3.2. Plasma-Catalytic Methane Cracking

3.2.1. Plasma and Plasma-Catalytic Test and Reaction Mechanism

The CH₄ cracking is undertaken for performance analysis of plasma and plasma-catalysis presented in Figure 7. The CH₄ conversion for plasma, MgAl₂O₄ and Ni/MgAl₂O₄ is recorded as 65%, 73% and 80% respectively at the same experimental conditions (Figure 7a). The plasma only CH₄ conversion is lower as compared to the plasma-catalytic reaction. Plasma only reaction occurs due to the electron-induced dissociation of CH₄, which is independent of reaction temperature [41]. The CH₄ molecules collide with an energetic electron in the plasma discharge zone at discharge volume (V_D) of 13.5 cm³ and start to dissociate while overcoming the required dissociation energy of 4.5 eV [22,42]. In plasma only electron-CH₄ interaction is induced, which led to the dissociation reactions and product formation reactions are as follows:

Dissociation reactions ((R2)–(R4))



Gaseous product formation reactions ((R5)–(R8))



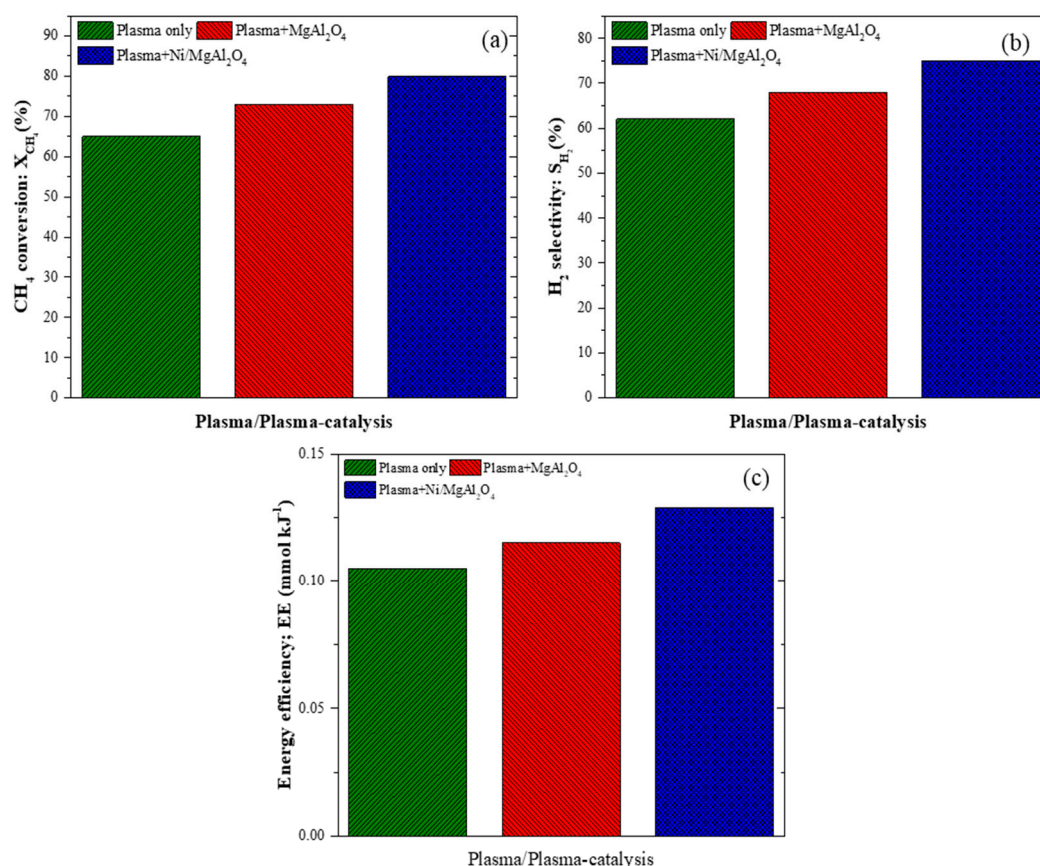


Figure 7. Plasma/plasma-catalyst activity: (a) X_{CH_4} conversion (b) S_{H_2} selectivity (c) EE; GHSV = 364 h^{-1} , specific input energy (SIE) = 300 J mL^{-1} , loading of catalyst = 0.5 g , $T = 350\text{ }^{\circ}\text{C}$, discharge gap (D_{gap}) = 03 mm , discharge length (D_L) = 20 cm , discharge volume (V_D) without catalyst: 13.5 cm^3 , V_D with catalyst loading = 9.75 cm^3 .

While loading the catalyst, CH_4 conversion is improving for $MgAl_2O_4$ (73%) and $Ni/MgAl_2O_4$ (80%). The catalyst loading improves the CH_4 conversion in both cases. In Ni loaded $MgAl_2O_4$ shows the highest conversion of CH_4 . The plasma produces hot spots on the catalyst, assist the Ni reduction, also changes catalyst functions, and reduce activation barrier due to gas heating effect [43]. While catalyst enriches the electric field, boost micro discharges and alters the discharge behaviour of DBD plasma. The catalyst-plasma interaction gives surplus effects called synergistic effect, which improves the conversion of CH_4 and EE of DBD catalytic reactor. The $MgAl_2O_4$ as a support material is mechanically stable and has porous structure confirmed by SEM, assist in activating CH_4 , and improve the DBD plasma discharge behaviour. Ni further assists the CH_4 activation due to active sites, activated by plasma give more surplus effect and enhanced the conversion by 15%. The plasma only and catalyst loaded DBD system shows the difference in the conversion of CH_4 and activity at certain level justifying by the synergistic effect. Unlike thermal catalysis, plasma-catalysis is not purely temperature dependent reaction. The energetic electron effect on the activation of reactant contributes more than catalytic effect [44]. However, the product selectivity in many cases is improved more as compare to conventional catalysis [45].

The H_2 and C_xH_x formation after the recombination of H^* and CH_x^* in governing steps [22]. The H_2 selectivity is noted 62% (Figure 7b), and some traces of C_2H_6 (1.5%) and C_2H_4 (1%) are also analysed in GC-FID for plasma only reaction. The H_2 selectivity of $MgAl_2O_4$ and $Ni/MgAl_2O_4$ is 68% and 75% respectively (Figure 7b). The enhanced H_2 selectivity is explained in the plasma-catalyst interaction mechanism. The undetected C_xH_x might be the balance for the H_2 and carbon balance in the product analysis due to the limitation of the analysis technique. The EE is lowest for plasma

only ($0.105 \text{ mmol kJ}^{-1}$) while MgAl_2O_4 ($0.115 \text{ mmol kJ}^{-1}$) and $\text{Ni/MgAl}_2\text{O}_4$ ($0.13 \text{ mmol kJ}^{-1}$) shows improvement in the EE due to the higher conversion of CH_4 at constant input power (Figure 7c). The combined effect of plasma and catalyst enhances the EE of the reaction, and hence it is suitable for CH_4 cracking in plasma-catalytic systems to improve EE over MgAl_2O_4 stable catalyst in mild conditions.

The proposed reaction mechanism for plasma-catalytic CH_4 cracking is demonstrated in Figure 8. It can be observed from the H_2 selectivity about the reaction mechanism. The activation of CH_4 to methyl radical CH_3^* and further breakdown in the presence of plasma while attachment to the metal (M, Ni). Similarly, further breakdown leads to the complete dissociation of the C-H bond to form C^* and H^* . While the recombination of H^* formed H_2 and released metal (M) [46]. At the same time, the traces of C_2H_6 has produced from the recombination of CH_3^* radicals. There are other possible routes for the formation of HCs, but the analysis of the product is more suitable for proposed pathways.

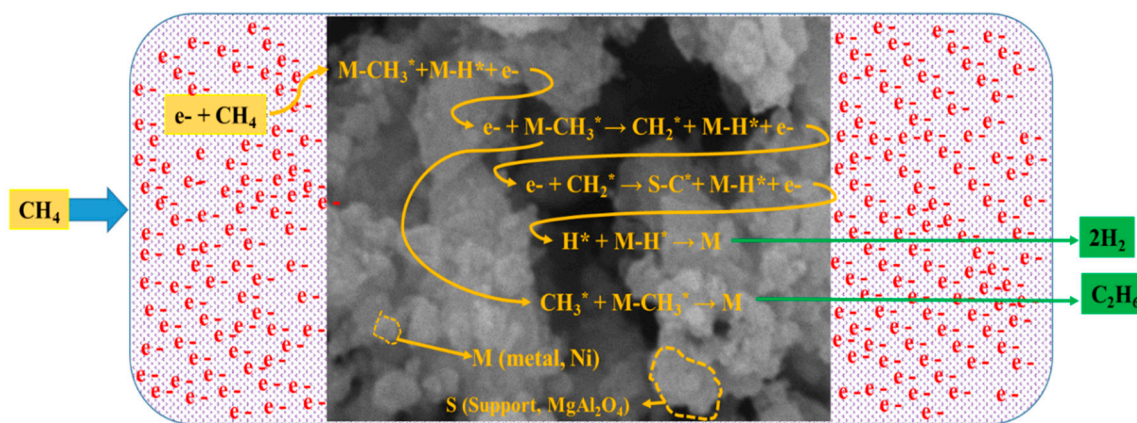


Figure 8. Proposed reaction mechanism for plasma-catalytic methane cracking over $\text{Ni/MgAl}_2\text{O}_4$.

3.2.2. Time on-Stream Analysis of $\text{Ni/MgAl}_2\text{O}_4$

The stability of the plasma-catalytic CH_4 cracking on $\text{Ni/MgAl}_2\text{O}_4$ catalyst is presented in Figure 9. The CH_4 conversion and H_2 selectivity being partially declining along with the TOS. The CH_4 conversion above 75% while sustaining the EE above $0.125 \text{ mmol kJ}^{-1}$. Along with the TOS the total reduction in the conversion of CH_4 , and H_2 selectivity is only -5% and -4% , respectively. The negative sign indicates the reduction in the conversion and selectivity. Similar trends can be observed for EE in the 16 h TOS. The stability is mostly attributed to the activation of NiO particles due to plasma species and instant heating. The impurities in the catalyst are also removed by plasma in catalyst expose to plasma [47]. The catalyst activation assists in the CH_4 activation as proposed in the possible reaction mechanism routes. Further, the breakdown of the methyl radical is also assisted by the plasma-catalyst interface while inhibiting the recombination of methyl radical, which is also observed the product analysis of in basic screening [43]. The plasma-catalyst interface improves many aspects since MgAl_2O_4 is mechanically stable support material and NiO also assist the Ni dispersion. The selectivity of H_2 is also ascribed to the highly basic nature of the MgAl_2O_4 , which improves the CH_x^* adsorption and assist in the activation and further breakdown [48–50]. The CH_4 cracking on plasma-catalytic to CH_x heavily depends on the $\text{Ni/MgAl}_2\text{O}_4$ interaction providing the higher coordinate sites in the plasma-catalytic interface, which is expected to achieve in the case for longer TOS. The plasma-catalytic interface gave reasonable stability and improved EE for CH_4 cracking in catalytic-DBD reactor condition.

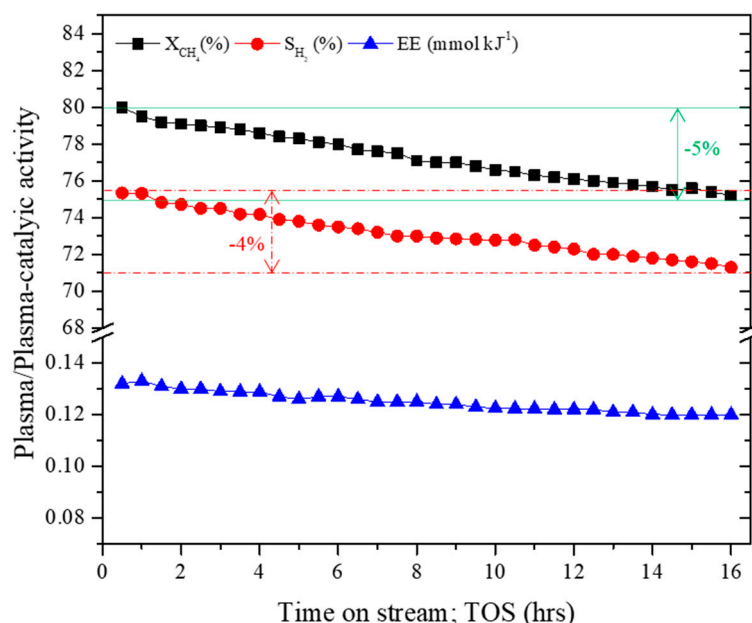


Figure 9. Analysis of time on stream (TOS) (16 h) on X_{CH_4} (%), S_{H_2} (%) and EE $mmol\ kJ^{-1}$. Experimental conditions: GHSV = $364\ h^{-1}$, specific input energy (SIE) = $300\ J\ mL^{-1}$, loading of catalyst = 0.5 g, $T = 350\ ^\circ C$, discharge gap (D_{gap}) = 03 mm, discharge length (D_L) = 20 cm, discharge volume (V_D) without catalyst: $13.5\ cm^3$, V_D with catalyst loading = $9.75\ cm^3$.

3.3. Characterisation of Spent Catalyst and Reaction Mechanism

The morphology and TGA-DTG analysis of the spent $Ni/MgAl_2O_4$ after 16 h TOS is given in Figure 10. The CNTs were observed in SEM analysis (Figure 10a) of spent catalyst along carbon fibres [51]. Mostly the CNTs formed are useful for further utilisation in energy storage application [31]. The TGA analysis (Figure 10b) shows the weight less than $200\ ^\circ C$ is ascribed to the volatile matters, while weight lost from 200 – $400\ ^\circ C$ is ascribed to the amorphous carbon. The weight loss beyond 500 is ascribed to the multiwall CNTs [52]. The CNTs can also be seen in SEM micrographs. The nature of the carbon formed is analysed using DTG profile (Figure 10b). The DTG curve at $355\ ^\circ C$, the peak is ascribed to the amorphous and fibrous carbon formed and ioxidized at less than $400\ ^\circ C$ [51]. The DTG curve at $690\ ^\circ C$ is ascribed to multiwall CNTs with low defects and low curvature with pure sp^2 structure [53,54]. The formed carbon is ascribed to a stable material for energy storage applications and discharge while increasing the temperature without surface modification [55]. This technology for methane cracking for simultaneous hydrogen and CNT formation is a beneficial process [56].

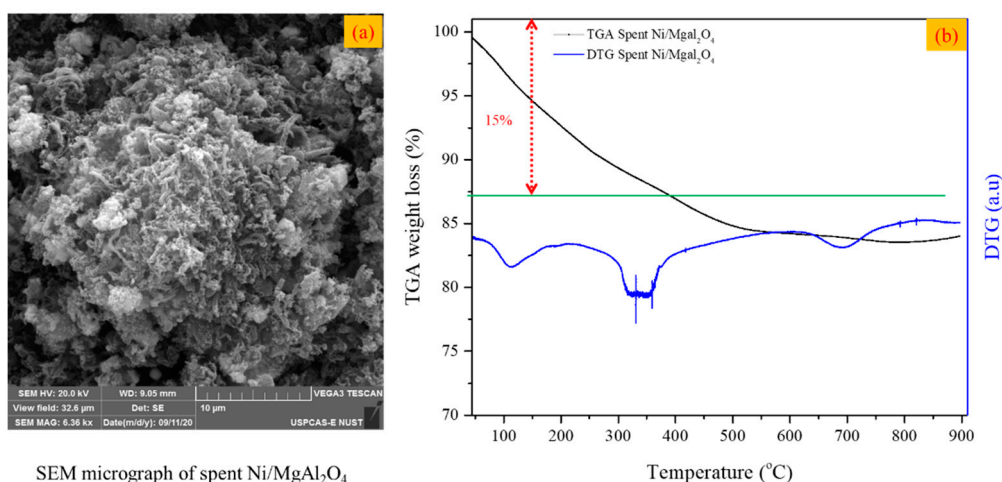


Figure 10. Spent Ni/MgAl₂O₄ after 16 h TOS analysis (a) SEM micrograph (b) TGA-DTG analysis.

4. Conclusions

The CH₄ cracking in catalytic DBD plasma fixed bed reactor has been studied and found that the plasma-catalytic process enhances the CH₄ conversion (80%), improved the EE of the catalytic DBD reactor. The possible interaction between plasma-catalyst enhances the discharge behaviour, active species and improve the contact time between electrons and gas molecules to dissociate and formed the products. The selectivity for H₂ is improved to 75% in plasma-catalytic-DBD systems as compared to plasma only CH₄ cracking (62%). While EE also improved in such manner 0.13 mmol kJ⁻¹. The 16 h TOS stability shows a slight declined in the CH₄ conversion due to the fibrous carbon and CNT formation confirmed from TGA-DTG analysis. The spent catalyst shows the formation of CNTs which are beneficial for further utilisation for energy storage systems.

The CH₄ utilisation in non-thermal DBD plasma for H₂ and CNTs formation is a highly desirable route for the simultaneous H₂ production and storage for fuel cell applications. Further study is recommended on the cleaning of H₂ in cold plasma catalytic systems via membrane or monolith reactor systems.

Author Contributions: Conceptualization, A.H.K. and N.A.S.A.; methodology, A.H.K. and M.T.M.; validation, A.K.A., S.R.N. and B.A.K.; formal analysis, A.H.K.; investigation, A.H.K.; N.A.S.A., writing—original draft preparation, A.H.K. and F.S.; writing—review and editing, A.K.A. and N.A.S.A.; supervision, N.A.S.A.; project administration and funding acquisition, A.H.K., N.A.S.A. All authors have read and agreed to the published version of the manuscript.

Funding: This research was funded by Universiti Teknologi Malaysia and the Ministry of Education, Malaysia for the financial support of this research under RUG (Research University Grant, Vot13H35) and FRGS-MRSA grant (Vot 4F988).

Acknowledgments: The authors appreciated Universiti Teknologi Malaysia and the (MOHE) Ministry of Education, Malaysia, for the financial support of this research.

Conflicts of Interest: The authors declare no conflict of interest.

References

- Goglio, R.; Smith, W.N.; Grant, B.B.; Desjardins, R.L.; Gao, X.; Hanis, K.; Tenuta, M.; Campbell, C.A.; McConkey, B.G.; Nemecek, T.; et al. A comparison of methods to quantify greenhouse gas emissions of cropping systems in LCA. *J. Clean. Prod.* **2018**, *172*, 4010–4017. [\[CrossRef\]](#)
- Salkuyeh, Y.K.; Adams, T.A. Combining coal gasification, natural gas reforming, and external carbonless heat for efficient production of gasoline and diesel with CO₂ capture and sequestration. *Energy Convers. Manag.* **2013**, *74*, 492–504. [\[CrossRef\]](#)
- Wang, X.; Gao, Y.; Zhang, S.; Sun, H.; Li, J.; Shao, T. Nanosecond pulsed plasma assisted dry reforming of CH₄: The effect of plasma operating parameters. *Appl. Energy* **2019**, *243*, 132–144. [\[CrossRef\]](#)

4. Schwietzke, S.; Sherwood, O.A.; Bruhwiler, L.M.; Miller, J.B.; Etiope, G.; Dlugokencky, E.J.; Michel, S.E.; Arling, V.A.; Vaughn, B.H.; White, J.W.; et al. Upward revision of global fossil fuel methane emissions based on isotope database. *Nature* **2016**, *538*, 88–91. [\[CrossRef\]](#)
5. Razi, F.; Dincer, I. A critical evaluation of potential routes of solar hydrogen production for sustainable development. *J. Clean. Prod.* **2020**, *264*, 121582. [\[CrossRef\]](#)
6. Khalifeh, O.; Taghvaei, H.; Mosallanejad, A.; Rahimpour, M.R.; Shariati, A. Extra pure hydrogen production through methane decomposition using nanosecond pulsed plasma and Pt-Re catalyst. *Chem. Eng. J.* **2016**, *294*, 132–145. [\[CrossRef\]](#)
7. Zhang, R.; Cao, Y.; Li, H.; Zhao, Z.; Zhao, K.; Jiang, L. The role of CuO modified La_{0.7}Sr_{0.3}FeO₃ perovskite on intermediate-temperature partial oxidation of methane via chemical looping scheme. *Int. J. Hydrogen Energy* **2020**, *45*, 4073–4083. [\[CrossRef\]](#)
8. Khoja, A.H.; Tahir, M.; Amin, N.A.S. Recent developments in non-thermal catalytic DBD plasma reactor for dry reforming of methane. *Energy Convers. Manag.* **2019**, *183*, 529–560. [\[CrossRef\]](#)
9. Khoja, A.H.; Anwar, M.; Shakir, S.; Mehran, M.T.; Mazhar, A.; Javed, A.; Amin, N.A.S. Thermal dry reforming of methane over La₂O₃ co-supported Ni/MgAl₂O₄ catalyst for hydrogen-rich syngas production. *Res. Chem. Intermed.* **2020**, *46*, 3817–3833. [\[CrossRef\]](#)
10. Lašič Jurković, D.; Liu, J.-L.; Pohar, A.; Likozar, B. Methane Dry Reforming over Ni/Al₂O₃ Catalyst in Spark Plasma Reactor: Linking Computational Fluid Dynamics (CFD) with Reaction Kinetic Modelling. *Catal. Today* **2020**. [\[CrossRef\]](#)
11. Dan, M.; Mihet, M.; Lazar, M.D. Hydrogen and/or syngas production by combined steam and dry reforming of methane on nickel catalysts. *Int. J. Hydrogen Energy* **2020**, *45*, 26254–26264. [\[CrossRef\]](#)
12. Snoeckx, R.; Bogaerts, A. Plasma technology—A novel solution for CO₂ conversion? *Chem. Soc. Rev.* **2017**, *46*, 5805–5863. [\[CrossRef\]](#) [\[PubMed\]](#)
13. Assad Munawar, M.; Hussain Khoja, A.; Hassan, M.; Liaquat, R.; Raza Naqvi, S.; Taqi Mehran, M.; Abdullah, A.; Saleem, F. Biomass ash characterization, fusion analysis and its application in catalytic decomposition of methane. *Fuel* **2021**, *285*, 119107. [\[CrossRef\]](#)
14. Pudukudy, M.; Yaakob, Z.; Takriff, M.S. Methane decomposition into CO_x free hydrogen and multiwalled carbon nanotubes over ceria, zirconia and lanthana supported nickel catalysts prepared via a facile solid state citrate fusion method. *Energy Convers. Manag.* **2016**, *126*, 302–315. [\[CrossRef\]](#)
15. Mendoza-Nieto, J.A.; Vera, E.; Pfeiffer, H. Methane Reforming Process by means of a Carbonated Na₂ZrO₃ Catalyst. *Chem. Lett.* **2016**, *45*, 685–687. [\[CrossRef\]](#)
16. Lašič Jurković, D.; Puliyalil, H.; Pohar, A.; Likozar, B. Plasma-activated methane partial oxidation reaction to oxygenate platform chemicals over Fe, Mo, Pd and zeolite catalysts. *Int. J. Energy Res.* **2019**, *43*, 8085–8099. [\[CrossRef\]](#)
17. Zhang, H.; Du, C.; Wu, A.; Bo, Z.; Yan, J.; Li, X. Rotating gliding arc assisted methane decomposition in nitrogen for hydrogen production. *Int. J. Hydrogen Energy* **2014**, *39*, 12620–12635. [\[CrossRef\]](#)
18. da Costa Labanca, A.R. Carbon black and hydrogen production process analysis. *Int. J. Hydrogen Energy* **2020**, *45*, 25698–25707. [\[CrossRef\]](#)
19. Nozaki, T.; Okazaki, K. Non-thermal plasma catalysis of methane: Principles, energy efficiency, and applications. *Catal. Today* **2013**, *211*, 29–38. [\[CrossRef\]](#)
20. Wang, B.; Cao, X.; Yang, K.; Xu, G. Conversion of methane through dielectric-barrier discharge plasma. *Front. Chem. Eng. China* **2008**, *2*, 373–378. [\[CrossRef\]](#)
21. Staffell, I.; Scamman, D.; Abad, A.V.; Balcombe, P.; Dodds, P.E.; Ekins, P.; Shah, N.; Ward, K.R. The role of hydrogen and fuel cells in the global energy system. *Energy Environ. Sci.* **2019**, *12*, 463–491. [\[CrossRef\]](#)
22. Taghvaei, H.; Jahanmiri, A.; Rahimpour, M.R.; Shirazi, M.M.; Hooshmand, N. Hydrogen production through plasma cracking of hydrocarbons: Effect of carrier gas and hydrocarbon type. *Chem. Eng. J.* **2013**, *226*, 384–392. [\[CrossRef\]](#)
23. Lee, H.; Lee, D.-H.; Song, Y.-H.; Choi, W.C.; Park, Y.-K.; Kim, D.H. Synergistic effect of non-thermal plasma-catalysis hybrid system on methane complete oxidation over Pd-based catalysts. *Chem. Eng. J.* **2015**, *259*, 761–770. [\[CrossRef\]](#)
24. Kim, S.-S.; Kim, J.; Lee, H.; Na, B.-K.; Song, H.K. Methane conversion over nanostructured Pt/γ-Al₂O₃ catalysts in dielectric-barrier discharge. *Korean J. Chem. Eng.* **2005**, *22*, 585–590. [\[CrossRef\]](#)

25. Indarto, A. Hydrogen production from methane in a dielectric barrier discharge using oxide zinc and chromium as catalyst. *J. Chin. Inst. Chem. Eng.* **2008**, *39*, 23–28. [\[CrossRef\]](#)
26. Son, I.H.; Kwon, S.; Park, J.H.; Lee, S.J. High coke-resistance MgAl_2O_4 islands decorated catalyst with minimizing sintering in carbon dioxide reforming of methane. *Nano Energy* **2016**, *19*, 58–67. [\[CrossRef\]](#)
27. Li, G.; Cheng, H.; Zhao, H.; Lu, X.; Xu, Q.; Wu, C. Hydrogen production by CO_2 reforming of CH_4 in coke oven gas over Ni–Co/ MgAl_2O_4 catalysts. *Catal. Today* **2018**, *318*, 46–51. [\[CrossRef\]](#)
28. Khoja, A.H.; Tahir, M.; Saidina Amin, N.A. Process optimization of DBD plasma dry reforming of methane over Ni/ La_2O_3 - MgAl_2O_4 using multiple response surface methodology. *Int. J. Hydrogen Energy* **2019**, *44*, 11774–11787. [\[CrossRef\]](#)
29. Guo, J.J.; Lou, H.; Zhao, H.; Chai, D.F.; Zheng, X.M. Dry reforming of methane over nickel catalysts supported on magnesium aluminate spinels. *Appl Catal A-Gen* **2004**, *273*, 75–82. [\[CrossRef\]](#)
30. Khoja, A.H.; Tahir, M.; Saidina Amin, N.A. Evaluating the Performance of a Ni Catalyst Supported on La_2O_3 - MgAl_2O_4 for Dry Reforming of Methane in a Packed Bed Dielectric Barrier Discharge Plasma Reactor. *Energy Fuels* **2019**, *33*, 11630–11647. [\[CrossRef\]](#)
31. Liu, W.; Yuan, H. Simultaneous production of hydrogen and carbon nanotubes from cracking of a waste cooking oil model compound over Ni-Co/SBA-15 catalysts. *Int. J. Energy Res.* **2020**. [\[CrossRef\]](#)
32. Charisiou, N.D.; Siakavelas, G.; Papageridis, K.N.; Baklavaridis, A.; Tzounis, L.; Avraam, D.G.; Goula, M.A. Syngas production via the biogas dry reforming reaction over nickel supported on modified with CeO_2 and/or La_2O_3 alumina catalysts. *J. Nat. Gas Sci. Eng.* **2016**, *31*, 164–183. [\[CrossRef\]](#)
33. Jamil, U.; Husain Khoja, A.; Liaquat, R.; Raza Naqvi, S.; Nor Nadyaini Wan Omar, W.; Aishah Saidina Amin, N. Copper and calcium-based metal organic framework (MOF) catalyst for biodiesel production from waste cooking oil: A process optimization study. *Energy Convers. Manag.* **2020**, *215*, 112934. [\[CrossRef\]](#)
34. Khoja, A.H.; Tahir, M.; Amin, N.A.S. Dry reforming of methane using different dielectric materials and DBD plasma reactor configurations. *Energy Convers. Manag.* **2017**, *144*, 262–274. [\[CrossRef\]](#)
35. Sanjabi, S.; Obeydavi, A. Synthesis and characterization of nanocrystalline MgAl_2O_4 spinel via modified sol–gel method. *J. Alloy. Compd.* **2015**, *645*, 535–540. [\[CrossRef\]](#)
36. Nishikawa, H.; Kawamoto, D.; Yamamoto, Y.; Ishida, T.; Ohashi, H.; Akita, T.; Honma, T.; Oji, H.; Kobayashi, Y.; Hamasaki, A.; et al. Promotional effect of Au on reduction of Ni(II) to form Au–Ni alloy catalysts for hydrogenolysis of benzylic alcohols. *J. Catal.* **2013**, *307*, 254–264. [\[CrossRef\]](#)
37. Wang, C.; Sun, N.; Zhao, N.; Wei, W.; Zhao, Y. Template-free preparation of bimetallic mesoporous Ni–Co–CaO– ZrO_2 catalysts and their synergetic effect in dry reforming of methane. *Catal. Today* **2017**, *281*, 268–275. [\[CrossRef\]](#)
38. Malekabadi, M.A.; Mamoori, R.S. Low-temperature synthesis of micro/nano Lithium Fluoride added magnesium aluminate spinel. *Ceram. Int.* **2018**, *44*, 20122–20131. [\[CrossRef\]](#)
39. Ray, D.; Reddy, P.M.K.; Subrahmanyam, C. Ni–Mn/ γ - Al_2O_3 assisted plasma dry reforming of methane. *Catal. Today* **2018**, *309*, 212–218. [\[CrossRef\]](#)
40. Wang, Q.; Cheng, Y.; Jin, Y. Dry reforming of methane in an atmospheric pressure plasma fluidized bed with Ni/ γ - Al_2O_3 catalyst. *Catal. Today* **2009**, *148*, 275–282. [\[CrossRef\]](#)
41. Heintze, M.; Pietruszka, B. Plasma catalytic conversion of methane into syngas: The combined effect of discharge activation and catalysis. *Catal. Today* **2004**, *89*, 21–25. [\[CrossRef\]](#)
42. Jiang, T.; Li, Y.; Liu, C.J.; Xu, G.H.; Eliasson, B.; Xue, B.Z. Plasma methane conversion using dielectric-barrier discharges with zeolite A. *Catal. Today* **2002**, *72*, 229–235. [\[CrossRef\]](#)
43. Khoja, A.H.; Tahir, M.; Amin, N.A.S. Cold plasma dielectric barrier discharge reactor for dry reforming of methane over Ni/ γ - Al_2O_3 - MgO nanocomposite. *Fuel Process. Technol.* **2018**, *178*, 166–179. [\[CrossRef\]](#)
44. Neyts, E.C.; Ostrikov, K.K.; Sunkara, M.K.; Bogaerts, A. Plasma catalysis: Synergistic effects at the nanoscale. *Chem. Rev.* **2015**, *115*, 13408–13446. [\[CrossRef\]](#) [\[PubMed\]](#)
45. Neyts, E.C.; Ostrikov, K. Nanoscale thermodynamic aspects of plasma catalysis. *Catal. Today* **2015**, *256*, 23–28. [\[CrossRef\]](#)
46. Yap, D.; Tatibouët, J.-M.; Batiot-Dupeyrat, C. Catalyst assisted by non-thermal plasma in dry reforming of methane at low temperature. *Catal. Today* **2018**, *299*, 263–271. [\[CrossRef\]](#)
47. Liu, C.J.; Li, M.Y.; Wang, J.Q.; Zhou, X.T.; Guo, Q.T.; Yan, J.M.; Li, Y.Z. Plasma methods for preparing green catalysts: Current status and perspective. *Chin. J. Catal.* **2016**, *37*, 340–348. [\[CrossRef\]](#)

48. Fan, Z.; Sun, K.; Rui, N.; Zhao, B.; Liu, C.-j. Improved activity of Ni/MgAl₂O₄ for CO₂ methanation by the plasma decomposition. *J. Energy Chem.* **2015**, *24*, 655–659. [[CrossRef](#)]
49. Guo, J.; Lou, H.; Zhao, H.; Zheng, X. Improvement of stability of out-layer MgAl₂O₄ spinel for a Ni/MgAl₂O₄/Al₂O₃ catalyst in dry reforming of methane. *React. Kinet. Catal. Lett.* **2005**, *84*, 93–100. [[CrossRef](#)]
50. Guo, J.; Lou, H.; Zheng, X. The deposition of coke from methane on a Ni/MgAl₂O₄ catalyst. *Carbon* **2007**, *45*, 1314–1321. [[CrossRef](#)]
51. Megía, P.J.; Calles, J.A.; Carrero, A.; Vizcaíno, A.J. Effect of the incorporation of reducibility promoters (Cu, Ce, Ag) in Co/CaSBA-15 catalysts for acetic acid steam reforming. *Int. J. Energy Res.* **2020**. [[CrossRef](#)]
52. Osman, A.I.; Blewitt, J.; Abu-Dahrieh, J.K.; Farrell, C.; Al-Muhtaseb, A.H.; Harrison, J.; Rooney, D.W. Production and characterisation of activated carbon and carbon nanotubes from potato peel waste and their application in heavy metal removal. *Env. Sci. Pollut. Res. Int.* **2019**, *26*, 37228–37241. [[CrossRef](#)] [[PubMed](#)]
53. Krishnia, L.; Kumari, R.; Kumar, V.; Singh, A.; Garg, P.; Yadav, B.S.; Tyagi, P.K. Comparative study of thermal stability of filled and un-filled multiwalled carbon nanotubes. *Adv. Mater. Lett.* **2016**, *7*, 230–234. [[CrossRef](#)]
54. Azmina, M.; Suriani, A.B.; Salina, M.; Azira, A.; Dalila, A.; Asli, N.; Rosly, J.; Nor, R.M.; Rusop, M. *Variety of Bio-Hydrocarbon Precursors for the Synthesis of Carbon Nanotubes*; Trans Tech Publisher: Baech, Switzerland, 2012; pp. 43–63.
55. Pudukudy, M.; Yaakob, Z.; Takriff, M.S. Methane decomposition over Pd promoted Ni/MgAl₂O₄ catalysts for the production of CO_x free hydrogen and multiwalled carbon nanotubes. *Appl. Surf. Sci.* **2015**, *356*, 1320–1326. [[CrossRef](#)]
56. Dong, Z.; Li, B.; Cui, C.; Qian, W.; Jin, Y.; Wei, F. Catalytic methane technology for carbon nanotubes and graphene. *React. Chem. Eng.* **2020**, *5*, 991–1004. [[CrossRef](#)]

Publisher's Note: MDPI stays neutral with regard to jurisdictional claims in published maps and institutional affiliations.



© 2020 by the authors. Licensee MDPI, Basel, Switzerland. This article is an open access article distributed under the terms and conditions of the Creative Commons Attribution (CC BY) license (<http://creativecommons.org/licenses/by/4.0/>).